On the Curvature Energy of a Thin Membrane Decorated by Polymer Brushes

T. M. Birshtein,[†] P. A. Iakovlev,[†,‡] V. M. Amoskov,[†] F. A. M. Leermakers,[*,‡] E. B. Zhulina,[†] and O. V. Borisov[†]

Institute of Macromolecular Compounds of the Russian Academy of Sciences, 199004 St. Petersburg, Russia, and Laboratory of Physical Chemistry and Colloid Science, Wageningen University, Dreijenplein 6, 6307 HB Wageningen, The Netherlands

Received June 12, 2007; Revised Manuscript Received October 25, 2007

ABSTRACT: In this work, we present approximate analytical predictions for the contribution to the free energy of curvature of a thin (flexible) membrane rising from a polymer brush, which is grafted to both sides of the membrane. The influence of the approximations is revealed by a detailed comparison with numerically exact self-consistent field (SCF) calculations. We consider both the quenched case, i.e., when the grafting density is the same on both sides, and the annealed case, i.e., when the polymer chains can translocate upon bending from one side of the membrane to the other. It is found that the analytical predictions give the correct sign for the brush contribution to the free energy of curvature. Moreover, for spherically curved membranes, a reasonably accurate scaling with the grafting density σ and the chain length N is obtained. However, in the case of a cylindrical curvature, the analytical models overestimate the dependence on the polymer chain length. It is shown that the mean bending modulus is positive, which implies that the grafting of polymers onto membranes makes these stiffer. The Gaussian bending modulus is negative and scales with the chain length in the power three, whereas the mean bending modulus scales with the chain length with a power two. This is in contrast with the analytical predictions which point to the same power-law dependence of three. Our results imply that for sufficiently long polymers the flat conformation becomes unstable in favor of bending.

Introduction

The investigation of the influence of a grafted polymer layer on the bending elasticity of a membrane has a long history. There are few issues that are commonly recognized. For example, it is clear that grafting of polymer chains on one side of a membrane would lead to a spontaneously curved conformation.[1,2] One may further argue that permanent grafting of an equal number of chains onto both sides of a membrane would both stabilize a flat conformation and increase the resistance against bending, i.e., such chains stiffen the bilayer. In this last example, it was taken that upon bending the chains cannot relocate from one side of a membrane to another. Such systems are referred to as quenched (with respect to chain redistribution through flop−flop).

At the same time, there are ample issues that are currently actively discussed in the literature. For example, the subtle question is what will happen with the stability and stiffness of a flat membrane when upon bending the grafted chains can redistribute from one side of the membrane to the other (see Figure 1). We refer to such a system as an annealed bilateral brush or, for simplicity, a bilateral brush. While the quenched state may be relevant in a fluctuating membrane at short time scales, the annealed one is of interest for equilibrated systems. Most experimental studies[3,4] as well as a some theoretical papers on polymer-decorated membranes[5,6] deal with self-organizing lipids partially coupled to polymer chains.[7,8] In this case of self-assembly, polymers are found on both sides of a membrane, and ideally their distribution is governed by the minimal free energy condition. Thus, the polymers can attain an asymmetric distribution in the curved regions of the membranes.[9] However, the extraction of the polymer contribution from the total free energy of the system is less straightforward here due to the polymer−lipid and lipid−lipid interactions.

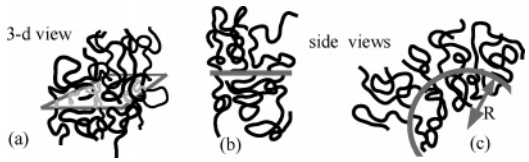

Figure 1. (a) A 3D schematic illustration of a flat bilateral brush. On both sides of the bilayer, the grafting density (i.e., the number of chains per unit area) is the same. (b) A side view of a cross-section of the bilateral brush. Again, on both sides one sees the same number of chains. (c) A section of the cross-section of a curved membrane with radius R. In this case, the number of chains on the concave side is less than the number of chains on the convex side, i.e., some chains have flipped or translocated. The view graph b can also be visualized as a line onto which the side chains are grafted (in 2D). Graph c can be viewed as a curved line. This illustrates that the curved bilateral brush is also a model for the curved molecular bottle-brush. In this work, we consider the supporting fluid membrane to be so flexible that its contribution to the overall rigidity can be ignored or, better stated, that the intrinsic flexibility of the supporting membrane should be added to the predictions elaborated below. Also, in this work, we focus on brushes with a laterally homogeneous grafting density.

The behavior of a bilateral brush system immersed in an athermal solvent was first studied by Birshtein and Zhulina.[10] The analysis was based on the Daoud−Cotton blob model for curved brushes[11] (see also[12,13]). Two bending modes, spherical and cylindrical, were considered. These two different membrane geometries allowed for the calculation of the polymer contributions to the mean and Gaussian bending rigidities. It was demonstrated that the bending of a membrane indeed leads to a redistribution of the chains from the concave side of the membrane to the convex one. At a large membrane curvature, the difference in chain redistribution for spherical and cylindrical

* To whom correspondence should be addressed. E-mail: frans.leermakers@wur.nl.
† Institute of Macromolecular Compounds of the Russian Academy of Sciences.
‡ Wageningen University.

10.1021/ma071303h CCC: $40.75
Published on Web 12/23/2007

types of bending is of solely quantitative character. In both spherical and cylindrical modes, the chains are accumulated on a convex side of a bending membrane, thus leading to the decrease in overall free energy per chain. At a weak curvature, the situation is more delicate. According to the blob model[10] and subsequent studies, the spherical bending always leads to a decrease in the total free energy per chain in a bilateral brush. At the same time, the cylindrical bending leads to an initial increase in the free energy per chain.[10] Therefore, in the framework of the blob model, at small curvatures of a membrane a spherical type of bending is favorable whereas the cylindrical bending is unfavorable. In terms of the membrane elasticity, this means that the polymer grafted to both sides of a membrane and being allowed to redistribute upon bending makes the membrane stiffer but less stable.

The observation that the sign of the effect depends on the type of bending demonstrates the delicacy of the problem, and this explains why so many issues in the field are still heavily debated. The small change in the free energy imposed upon a curvature results from subtracting two large numbers (the free energies of the curved and the flat membrane conformations). Meanwhile, the analytical theory contains invariably a number of approximations. In particular, the results in ref 10 were based on the assumption that all the free polymer ends are fixed at the external boundary of a brush. At first sight this assumption seems reasonable as it is similar to the approximation made in, e.g., the classical Alexander-de Gennes box model for flat brushes[14,15]. Another approximation inherent for the Daoud−Cotton blob model[10] is the so-called quasi-planar approximation (QP).[16] In this framework, the local structure in a curved brush at distance r from the membrane coincides with that in a planar brush with r-dependent grafting area per chain. As a result, the polymer density profile in a curved brush is unaffected by the peripheral parts of the brush. It is described by a power law which is independent of molecular weight of the grafted chains.

For almost two decades, the Daoud−Cotton blob model[11] served as the main tool to rationalize the experimental data on curved brushes and related systems (polymer-decorated colloids, solutions of starlike polymers, block copolymer aggregates of various morphologies, etc.). A recent revision of this model[16] indicated that although the quasi-planar approximation has the adequate asymptotic power laws for the average brush thickness and the free energy, it fails to predict correctly the polymer density and lateral tension distribution profiles in curved brushes. A more accurate calculation of these characteristics is possible by direct minimization of the free energy, which indicates that the local brush structure is affected by the brush peripheral parts, and therefore the distributions of the polymer density and the lateral tension depend on the molecular weight of the chains (see ref 16 for details). Therefore, the local features in the brush are determined by the overall spatial distribution of the polymer. This model is therefore referred to as having the nonlocal (NL) approximation. In this framework, the polymer density profile does not obey a power law, the chains are more stretched, and more polymer material is expelled to the periphery of a convex brush. The difference between the two frameworks (QP and NL) becomes quite noticeable for charged grafted chains. For a neutral polymer brush, which is the focus of this paper, the difference between outputs of the two models is relatively small. However, due to the delicacy of the bilateral brush behavior at small curvatures, the nonlocal effects can contribute to the overall behavior of the bilayer. We therefore believe that it is timely to try to understand the thermodynamics of bending of a bilateral brush using up-to-date considerations for the structural organization of curved brushes.

An important class of polymers directly relevant to the topic of this study comprises the so-called molecular brushes or comblike macromolecules.[17−23] When such macromolecules adsorb onto a strongly attractive substrate, they become effectively two-dimensional. Locally, the conformations of an adsorbed molecular brush can be envisioned as a cross-section of a cylindrically curved three-dimensional bilateral brush (see Figure 1). The interactions between the side chains stiffen the macromolecule, and this determines its adsorption-induced persistence length. For a quenched system with prohibited redistribution of side arms from one side of the molecular backbone to the other, the straight configuration of the macromolecule is thermodynamically stable and the optimal one, in this case the persistence length, is large. For an annealed system (two-dimensional bilateral brush), the flip−flop of side chains leads to a smaller persistence length, and this can even cause a spontaneous curvature in adsorbed comblike macromolecules.[24,25] The latter theoretical prediction turned out to be model dependent and is challenged by the results in ref 23. Overall, the current understanding of a molecular brush behavior is far from being complete.

The aim of this work is therefore to present the most accurate analytical predictions available up-to-date for the free energy change due to the bending of a planar bilateral brush. Both the limits of weak and strong membrane curvature in spherical and cylindrical modes will be considered, and the bending and the Gaussian moduli will be analyzed. The results will be critically compared to the predictions of the numerically exact Scheutjens−Fleer self-consistent field (SF-SCF) method. From this comparison, we will derive the conclusions regarding the accuracy of the analytical models as well as what must be expected in experimental systems.

The remainder of the paper is organized as follows. In the next part, we present an outline of the SF-SCF approach. It is followed by the presentation of the analytical theory, which includes two subparts; the analysis of weakly curved brushes with emphasis on the quasi-planar and the nonlocal approximations followed by the predictions for a curved bilateral brush. In the results section, we will present and discuss our numerical data. The summary of our conclusions is presented at the end of the paper.

Numerical SCF Method

For the most accurate evaluation of the free energy of bending we use the SF-SCF approach.[26−29] The target of these calculations is to find the structural and thermodynamic properties of the system that optimizes its free energy. As a result of the calculations, both the end-grafted chains and their free ends occupy the most favorable positions. Therefore, this model does not suffer from the assumptions that the free ends are constrained to the edge of the brush. All possible and allowed conformations of the chains are included, and therefore it also automatically includes the nonlocal contributions discussed below. Due to the model, which will be discussed below, the calculations also account rigorously for the redistribution of chains from one side of a membrane to another, and thus the calculations are ideally suited to the annealed brush system, i.e., the bilateral brush.

The SF-SCF approach is based on mean-field and lattice approximations. In this method, the space is taken to be composed of lattice sites with characteristic length l and the volume per cell is fixed at $\upsilon \propto l^3$. The lattice sites are arranged in layers numbered $r = 1, \cdots, M$. The number of lattice sites in

each layer, $L(r)$, depends on the geometry. For a flat lattice, this number does not depend on r, and $L(r) = L = L_x \times L_y$. In a cylindrical coordinate system, the number of sites in the radial direction is $L(r) \propto rL_x$ when the long axis of the cylinder is in the x direction. In the spherical coordinate system $L(r) \propto r^2$, where in the last two cases $r = 1$ is the central layer. Typically, we will impose reflecting (mirrorlike) boundary conditions in the lattice, although for the spherical and cylindrical geometries the natural boundary condition at $z = 0$ is that there are no lattice sites at this coordinate (no place for any molecules).

We consider polymer chains in a good or θ ($\chi = 0.5$) monomeric solvent. The solvent molecules are assumed to occupy one lattice site each. A chain is divided into N segments and numbered $s = 1, \cdots, N$. A polymer segment is also assumed to fit exactly on one lattice site. All dimensions are thus represented in units, $l \approx 0.5$ nm, of the lattice site length. As usual, all energies are expressed in units of k_BT.

In the bilateral brush model, we graft the polymers with their first segment $s = 1$ to a given coordinate $R \equiv r_g$. In this case, all polymers are free to take all possible r positions, i.e., $r \leq R$ as well as $r \geq R$. Typically, we choose $M \gg R \gg 1$, and the chains are grafted far from the system boundary. However, when the brushes are highly curved, it may be the case that R is not far from $r = 1$ and then the "inner" space becomes limited. This spatial confinement is, in such cases, accurately accounted for in the calculations. The mean curvature of the grafted layers in the cylindrical and spherical coordinate systems is given by $J = 1/R$ and $J = 2/R$, respectively. We can also study the characteristics of quenched convex or concave brush layers separately. In this case, the grafting surface R is taken to be impermeable. In the concave system, only the space $r < R$ is available for the chains, whereas in the convex problem, the other half-space $r > R$ is used. In this quenched system, it is possible to mimic the redistribution of the chains from one side of the membrane to another only by varying the grafting density (number of grafted chains per unit area) σ on both sides of the grafting plane, calculate the free energy as a function of $\Delta\sigma$ ($\sigma_{convex} \equiv \sigma_+ = \sigma + \Delta\sigma$; $\sigma_{concave} \equiv \sigma_- = \sigma - \Delta\sigma$), and then minimize it with respect to $\Delta\sigma$.

Again, the SCF calculations are optimizing the polymer conformations so that the free energy is minimal. The allowed conformations are generated using a Markov approximation. This means that only the correlations between the neighboring segments are included. This results automatically in a freely jointed chain model. The optimization is done by solving the Edwards diffusion equation:

$$\frac{\partial G(z,N)}{\partial N} = \frac{1}{6}\nabla G(z,N) - u(z)G(z,N) \quad (1)$$

where the ∇ operator is different for the various geometries. Eq 1 must be complemented with appropriate boundary and starting conditions. Here, $G(r,N)$ is a chain weighting factor which is related to the single chain partition function $G(N) = \sum_r L(r)G(r,N)$ and thus to the volume fraction distributions. The self-consistent segment potential $u(r)$ is given by

$$u(r) = -\ln(1 - \varphi(r)) - 2\chi\langle\varphi(r)\rangle \quad (2)$$

where φ is the polymer volume fraction. Here χ is the well-known Flory−Huggins interaction parameter. The angular brackets represent a three-layer average similarly as used below. The volume fraction profile of the solvent $\varphi_S(r)$ is found from the incompressibility constraint: $\varphi_S(r) = 1 - \varphi(r)$.

On the lattice, the eq 1 transforms into a set of propagator equations, which provides a very efficient way to evaluate the volume fractions. We will illustrate the equations with the bilateral brush in mind. In this formalism, the polymer volume fractions are found by the so-called composition law:

$$\varphi(r) = \sum_{s=1}^{N} \varphi(r,s) = \frac{\sigma L(R)}{G(N)} \sum_{s=1}^{N} \frac{G(r,s|R,1)G(r,s|N)}{G(r)} \quad (3)$$

where we have introduced a slight modification to the notation of the chain weighting factor to clarify that the grafting condition has broken the inversion symmetry in the chain statistics. The segment weighting factor is given by the Boltzmann weight $G(r) = \exp -u(r)/k_BT$. The chain weighting factor $G(r,s|R,1)$ is found with the forward propagator, whereas the complementary one $G(r,s|N)$ is found with the backward propagator. The forward propagator starts with $G(R,1|R,1) = G(R)$ and $G(r,1|r,1) = 0$ for $r \neq R$. Then,

$$G(r,s|R,1) = G(r) \sum_{r'=r-1,r,r+1} G(r',s-1|R,1)\lambda(r',r) \equiv G(r)\langle G(r,s-1|R,1)\rangle \quad (4)$$

wherein the a priori step probabilities obey the internal balance equation $L(r)\lambda(r,r') = L(r')\lambda(r',r)$ and give the (lattice-type and geometry-dependent) probability to step from layer r to r'. They further obey the constraint $\sum_{r'} \lambda(r',r) = 1$. The rhs of eq 4 defines the angular bracket notation already used in eq 2 for the weightage of the volume fractions. The backward propagator is started by the unconstrained end of the chain, and therefore $G(r,N|N) = G(r)$ for all r and reads

$$G(r,s|N) = G(r) \sum_{r'=r-1,r,r+1} G(r',s+1|N)\lambda(r',r) \quad (5)$$

where it is understood that the single chain partition function in this case is connected to the forward propagator $G(N) = \sum_r L(r)G(r,N|R,1)$.

As already mentioned, the potentials (u) depend on the volume fractions and the latter in turn are a function of the potentials. A self-consistent solution is routinely found numerically with a high precision. For such a solution, it is possible to evaluate the free energy accurately. Of interest is the free energy in units of k_BT per unit area measured at the grafting plane at which there are $L(R)$ site:

$$F \equiv \frac{F}{L(R)} = \sigma \ln \frac{\sigma L(R)}{G(N)} + \sum_r L(r) \ln(1 - \varphi(r)) + \sum_r L(r)\varphi(r)\chi\langle\varphi(r)\rangle \quad (6)$$

Below we compare the results of these calculations with the those of the analytical theories.

Analytical Theory

Theory for Curved Brushes. The overall characteristics of a polymer brush, its thickness H_d and free energy F_d, are related to the segment density $\varphi(r)$ and free energy density $f[\varphi(r)]$. Here we introduce the subindex d as the geometry index ($d = 1$ for a flat plane, $d = 2$ for the cylindrically curved layer, and $d = 3$ for the spherical geometry). We can write the free energy as

$$F_d^{\pm} = \pm\frac{1}{R^{d-1}} \int_R^{R\pm H_d} f[\varphi(r)]r^{d-1}\,dr \quad (7)$$

It is clear that the integration over the volume fraction profile should conserve the number of segments in the chain and thus should obey the constraint

$$N = \pm\frac{1}{\sigma_{\pm}R^{d-1}}\int_{R}^{R\pm H_d}\varphi(r)r^{d-1}\,\mathrm{d}r \tag{8}$$

Again, we have used R as the curvature radius of a grafting surface, the indexes (+) and (−) represent the outer and inner sides of a curved surface, and σ_+ and σ_- are the grafting densities of the polymers on the corresponding sides. In eq 7, the free energy is calculated for a unit of surface area, and we will refer to it as the specific free energy of the brush. This free energy must be directly compared to the SF-SCF result given in eq 6.

The task is to find a minimum in $F_d^{\pm}$ taking the constraint of eq 8 into account. Unfortunately, the rigorous analytical solution for the distribution of the free ends of the polymer (which is related to the single chain partition function) is not possible for curved convex brushes; it is only available numerically (SF-SCF) as mentioned above. The common Ansatz for analytical considerations is to assume that all the free ends are located at a certain distance from the grafting plane, i.e., exactly at the brush thickness H_d. This approximation implies that all the chains in the brush are equally stretched. We note that for polymer chains in curved geometries the local stretching along the chain is known to be different in different parts of the brush. The area per chain or, equivalently, the effective grafting density in each thin cylindrical or spherical layer depends on the coordinate r as:

$$\sigma(r) = \sigma_{\pm}\left(\frac{R}{r}\right)^{\pm(d-1)} \tag{9}$$

The minimization of the free energy of eq 7 with respect to $\varphi(r)$ (and taking into account the constrain 8) leads to the following equation:

$$\frac{\partial f(\varphi(r))}{\partial\varphi(r)} = \lambda \tag{10}$$

where λ is an indefinite Lagrange multiplier. As could be seen from eq 10), we can interpret λ as an exchange chemical potential, "polymer−solvent", which must remain constant throughout the brush. λ should also provide the equilibrium between the brush boundary and the solvent, which is equivalent to the minimum of the free energy per polymer segment at the boundary (or equal to zero chemical potential of the solvent).

$$\left.\frac{\partial\left(\dfrac{f(\varphi(r))}{\varphi(r)}\right)}{\partial\varphi(r)}\right|_{r=R\pm H_d} = 0 \tag{11}$$

The eqs 2−11 can be used to solve for the brush characteristics for a given imposed radius R, a chain length N, and a grafting density σ. For curved brushes, eqs 10 and 11 provide the polymer concentration distribution $\varphi(r)$ depending on the conditions at the brush boundary. Following the recent work,[14] where a similar theory was presented for curved brushes, we call this approach the nonlocal (NL) theory. For flat brushes these equations lead to the well-known box model with a constant polymer density φ in the brush, and the free energy density is represented as:

$$f(\varphi) = \frac{3}{2}\frac{\sigma^2}{\varphi} + f_{\mathrm{int}}(\varphi) \tag{12}$$

with $\varphi = N\sigma/H_1$.

The first term in eq 12 accounts for the free energy of stretching of a Gaussian chain, and the second is responsible for the free energy of chain interactions. In this work, we restrict ourselves to the case of uncharged layers in a good or θ solvent. In this case

$$f_{\mathrm{int}} = \begin{cases} \upsilon\varphi^2 & \text{good solvent} \\ \omega\varphi^3 & \theta \text{ solvent} \end{cases} \tag{13}$$

Here υ and ω are the dimensionless second and third virial coefficients for the segment interactions, which we set equal to unity. In eqs 12−13, we follow Flory[30] by using the mean-field Ansatz in that the probability of pair interactions is proportional to φ^2.

Minimizing eq 12 with respect to φ, we obtain the well-known scaling expressions:

$$\varphi = \begin{cases} \sigma^{2/3} & \text{good solvent} \\ \sigma^{1/2} & \theta \text{ solvent} \end{cases} \tag{14}$$

$$H_1 = \begin{cases} N\sigma^{1/3} & \text{good solvent} \\ N\sigma^{1/2} & \theta \text{ solvent} \end{cases} \tag{15}$$

$$F_1 = \begin{cases} N\sigma^{5/3} & \text{good solvent} \\ N\sigma^{2} & \theta \text{ solvent} \end{cases} \tag{16}$$

We will use these characteristics of the flat brush, $H_1$and F_1, (instead of N and σ) as a starting (reference) point. Note that a useful measure of the curvature for a nonplanar brush is given by H_1/R.

It should be possible to see the weakly curved brushes to be slightly perturbed with respect the flat brush and that the corrections can be written in series expansion with respect to this small parameter H_1/R. The NL theory for convex brushes[14] gives the result of the free energy for a weakly curved convex brush as

$$F_d^{+} = F_1\left[1 - a_{1d}\left(\frac{H_1}{R}\right) + a_{2d}\left(\frac{H_1}{R}\right)^2 + \cdots\right] \tag{17}$$

The coefficients a_{1d} and a_{2d} taken from ref 14 are presented in Table 1 (the values of a_{1d} and a_{2d} that were derived using the quasi-planar (QP) approximation are presented in this table as well). In the QP approximation, each layer of a brush is taken to be in equilibrium with the solvent, i.e., eq 11 is obeyed for each r, and the density of the brush in layer r is defined by eq 14 with the factor σ substituted by $\sigma(r)$ as shown in eq 9:

$$\varphi(r) = \begin{cases} (\sigma(r))^{2/3} & \text{good solvent} \\ (\sigma(r))^{1/2} & \theta\text{−solvent} \end{cases} \tag{18}$$

As a result, according to the QP approximation, the free energy expansion for weakly curved brushes can be presented in a general form for both the concave (F_d^{+}) and the convex (F_d^{-}) brushes with the same coefficients as:

$$F_d^{\pm} = F_1\left[1 \mp a_{1d}\left(\frac{H_1}{R}\right) + a_{2d}\left(\frac{H_1}{R}\right)^2 \mp \cdots\right] \tag{19}$$

It follows from Table 1 that both approximations lead to similar coefficients for the linear term. The coefficients a_{2d} however have different forms for the two approximations, but the numerical difference is small.

In Table 1, we have also included the coefficients a_{1d} and a_{2d} that were calculated in the early work of Birshtein et al.[6] for the good solvent case using the QP approximation but taking

Table 1. Coefficients of Expansion of Free Energy of the Curved Brush (Eq 19) for the Nonlocal (NL), Quasi-planar (QP), and Quasi-planar with Correlations (QP′) Analytical Models

regime	approach	a_1	a_2	a_2 ($d = 2$)	a_2 ($d = 3$)
good solvent	NL	$(d-1)/3$	$(d-1)(2d+1)/27$	0.18	0.52
	Qp	$(d-1)/3$	$d(d-1)/9$	0.22	0.67
	QP′	$(512)(d-1)$	$5/216(d-1)(7d-1)$	0.30	0.93
θ solvent	NL	$(d-1)/3$	$(d-1)(5d-1)/24$	0.37	1.17
	QP	$(d-1)/2$	$(d-1)(3d-1)/12$	0.42	1.33

into account the correlation corrections. Such correlation corrections are possible with the scaling approximation wherein the probability of pair interactions is proportional to $\varphi^{9/4}$ or, by equivalent, the free energy per blob is equal to k_BT.[31] These results are denoted in Table 1 by QP′.

For the general case of an arbitrarily curved brush, we will present equations only in the QP approximation. According to eqs 7 and 8 and also taking into account eqs 9, 14, and 18, we obtain for the conservation of segments in the chain

$$N = \begin{cases} \pm\dfrac{3}{d+2}\dfrac{R}{\sigma_\pm^{1/3}}\left(\left(\dfrac{R \pm H_d}{R}\right)^{(d+2)/3} - 1\right) & \text{good solvent} \\ \pm\dfrac{2}{d+1}\dfrac{R}{\sigma_\pm^{1/2}}\left(\left(\dfrac{R \pm H_d}{R}\right)^{(d+1)/3} - 1\right) & \theta \text{ solvent} \end{cases} \tag{20}$$

and for the free energy of the curved brush

$$F_d^\pm = \begin{cases} \pm\dfrac{3}{4-d} R\sigma_\pm^{4/3}\left(\left(\dfrac{R \pm H_d}{R}\right)^{(4-d)/3} - 1\right) & \text{good solvent} \\ \pm\dfrac{2}{3-d} R\sigma_\pm^{3/2}\left(\left(\dfrac{R \pm H_d}{R}\right)^{(3-d)/3} - 1\right) & \theta \text{ solvent, } d \neq 3 \\ \pm R\sigma_\pm^{3/2}\ln\left(\dfrac{R \pm H_d}{R}\right) & \theta \text{ solvent, } d = 3 \end{cases} \tag{21}$$

In eq 21 (and below), there are two different equations for the θ-solvent case, one for the $d \neq 3$ and the other for $d = 3$. Using H_1 and F_1 of eqs 15 and 16 as parameters, we then get from eqs 20 and 21

$$F_d^\pm = \begin{cases} \pm\dfrac{3}{4-d}\dfrac{R}{H_1}F_1\left(\left(1 \pm \dfrac{d+2}{3}\dfrac{H_1}{R}\right)^{(4-d)/(2+d)} - 1\right) & \text{good solvent} \\ \pm\dfrac{2}{3-d}\dfrac{R}{H_1}F_1\left(\left(1 \pm \dfrac{d+1}{2}\dfrac{H_1}{R}\right)^{(3-d)/(1+d)} - 1\right) & \theta \text{ solvent, } d \neq 3 \\ \pm\dfrac{1}{2}\dfrac{R}{H_1}F_1\ln\left(1 \pm 2\dfrac{H_1}{R}\right) & \theta \text{ solvent, } d = 3 \end{cases} \tag{22}$$

$H_1$and F_1 in these formulas are functions of $\sigma_\pm$. Series expansion of eq 22 with respect to H_1/R can be casted in the form of eq 19 with coefficients presented in the QP row of Table 1.

The Curvature Free Energy of a Bilateral Brush. We now consider the change in the specific free energy when a flat bilateral brush is curved, i.e., the free energy of bending of the bilateral brush, in such a way that the chains can translocate. When the flat membrane is homogeneously bent, the outcome is a cylindrical or spherical object with radius R. In this process, the area is conserved, i.e., we assume that the flat membrane splits up into various parts and that each part is subsequently bent into the specified object.

As long as the bilayer is flat, we assume that both sides of the membrane are covered by the same number of grafted chains. The overall grafting density is fixed upon bending; however, the grafting density on either side of the bilayer is allowed to change. The translocation of chains that is necessary for this is sometimes referred to by the flip or flip−flop of chains. It is clear that when this relaxation mechanism is available for a system, it will be used to lower its free energy. The number of flips that is chosen in a particular case will be controlled by the minimum of the free energy. In this way

$$\sigma_\pm = (1 \pm x)\sigma \tag{23}$$

where $x = \Delta\sigma/\sigma$. The relative change in the specific free energy upon bending can be written as

$$\delta F = \frac{\Delta F}{F_1} = \frac{F_d^+ + F_d^- - 2F_1}{F_1} = \frac{F_d}{A_d} - 2 \tag{24}$$

where according to eqs 16 and 22−24

$$F_d = \begin{cases} \dfrac{2+d}{4-d}\{(1+x)^{4/3}(B_{d+}^{(4-d)/(2+d)} - 1) + (1-x)^{4/3}(1 - B_{d-}^{(4-d)/(2+d)})\} & \textit{good solvent} \\ \dfrac{1+d}{2-d}\{(1+x)^{3/2}(B_{d+}^{(3-d)/(1+d)} - 1) + (1-x)^{3/2}(1-x)^{3/2}(1 - B_{d-}^{(3-d)/(1+d)})\} & \theta \text{ solvent, } d \neq 3 \\ (1+x)^{3/2}\ln B_{d+} - (1-x)^{3/2}\ln B_{d-} & \theta \text{ solvent, } d = 3 \end{cases} \tag{25}$$

Table 2. Coefficients in the Expansion of Key Characteristics of the Bilateral Brush, Equations 29 and 30, for the Nonlocal (NL), Quasi-planar (QP), and Quasi-planar with Correlations (QP′) Analytical Models

regime	approach	b_1	b_2	b_2 ($d = 2$)	b_2 ($d = 3$)
good solvent	NL	$(3/5)(d-1)$	$0.25(d-1)(1.88-d)$	−0.030	−0.56
	QP	$(3/5)(d-1)$	$0.18(d-1)(2.25-d)$	0.045	−0.27
	QP′	$(13/22)(d-1)$		0.068	−0.28
θ solvent	NL	$(5/8)(d-1)$	$0.36(d-1)(1.91-d)$	−0.032	−0.78
	QP	$(5/8)(d-1)$	$0.28(d-1)(2.18-d)$	0.050	−0.45

Quantities A_d and B_d for different solvent strengths are given by

$$A_d = \begin{cases} \dfrac{d+2}{3}\dfrac{H_1}{\mathrm{R}} = \dfrac{\mathrm{d}+2}{3}\dfrac{N\sigma_{\pm}^{1/3}}{R} & \text{good solvent} \\ \dfrac{d+2}{3}\dfrac{H_1}{R} = \dfrac{d+2}{3}\dfrac{N\sigma_{\pm}^{1/2}}{R} & \theta \text{ solvent} \end{cases} \tag{26}$$

$$Bd_{\pm} = \begin{cases} 1 + A_d(1 \pm x)^{1/3} & \text{good solvent} \\ 1 \pm A_d(1 \pm x)^{1/2} & \theta \text{ solvent} \end{cases} \tag{27}$$

In this problem, we need to minimize the free energy (eq 25) with respect to the x variable:

$$\frac{\mathrm{d}F_d}{\mathrm{d}x} = 0 \tag{28}$$

which gives the equilibrium values for x and δF at given values of d and A_d.

Using eq 19, we obtain the first terms of the expansion in the weak curvature limit: and

$$x = b_1\left(\frac{H_1}{R}\right) \tag{29}$$

$$\delta F = b_2\left(\frac{H_1}{R}\right)^2 \tag{30}$$

Here b_1 and b_2 are numerical coefficients, b_1 is proportional to the coefficient a_{1d} of the free energy expansion given in eq 19, and b_2 depends on two coefficients a_{1d} and a_{2d} of this expansion. The b_1 and b_2 coefficients for all cases in eqs 29 and 30 are presented in Table 2. The calculation of coefficients in the NL model, similar to calculation in QP models, was based on eq 19. Note that from ref 14 we know the theoretical coefficients a_1 and a_2 only for the convex brush (cf. eq 17).

From Table 2, one can see that the values of the b_1 coefficient are the same for both QP and NL approximations. The value of the b_2 coefficient used in eq 30 is more delicate. As follows, from the expansion of eq 19 and eqs 24 and 28, the b_2 coefficient is found by the difference between a_2 and a term that depends on a_1 (or b_1). As a result, we find that for spherical bending ($d = 3$) this difference (b_2) is always negative, whereas for cylindrical bending the sign of the b_2 value is model dependent. Indeed, according to the QP and QP′ models, b_2 for cylindrical bending is positive, which is in line with the early predictions.[6] The positive value indicates that the curvature free energy for weak cylindrical bending is unfavorable. This is in contrast to the prediction of the NL model, where $b_2 < 0$ for both the spherical and the cylindrical bending cases (Table 2).

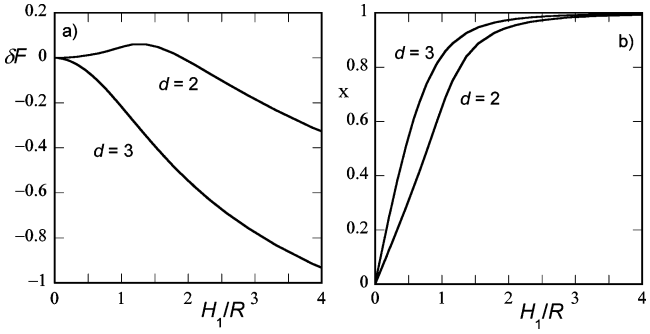

Figure 2. (a) The relative change in the specific free energy upon bending δF using the QP approximation, see eqs 24−28, and (b) the fraction of translocated chains x as a function of relative curvature H_1/R for spherical ($d = 3$) and cylindrical ($d = 2$) curvatures. The initial grafting density per side is $\sigma = 0.1$, and the solvent quality is good ($\chi = 0$).

Up to this point, we have limited ourselves to the weakly curved regime. The dependence of x and δF on H_1/R for a large range of R values is presented in Figure 2 for the QP model. In this graph, it is seen that δF changes sign upon curvature in the cylindrical geometry. It is positive for the weak curvature and becomes negative at larger curvatures. For the spherical curvature, we find δF to be negative for all values of the imposed radius R. Interestingly, the physically more correct NL model predicts monotonically decreasing values for δF in both geometries. These results are in accordance with the signs of b_2 presented in Table 2. In all cases, δF turns negative when H_1/R becomes large, i.e., when R becomes small. Thus the extreme curvatures are always favorable. It is relatively easy to understand this effect. In the limit of very high H_1/R, most of the polymers will be on the exterior side of the membrane as x tends to unity. Taking the spherical bending as an example, one is left with a very small sphere of radius R decorated with end-grafted chains with a grafting density of 2σ. That means that the number of chains at the surface $n = 8\pi R^2\sigma$ is also small. These chains become so dilute that they do not interact, i.e., do not stretch each other.

The results of analytical considerations presented in this part of the article serve as a guide for the numerical SF-SCF analysis presented in the next section. Equations 29 and 30 and Figure 2 show that there are two scaling parameters. The free energy of the curved brush is proportional to the free energy of the planar brush, which is proportional to N (cf. eq 16), while the natural measure of the curvature is H_1/R, which is also proportional to N (cf. eq 15). The scaling as obtained in the QP model also applies to the NL approximation because, according to Zhulina and Birshtein,[14] a shift from the QP to the NL approximation does not affect the scaling relationships for convex brushes; it changes only the numerical coefficients (see Table 1).

As follows, from eqs 15, 16, 24, and 30, the predicted scaling dependencies for the initial part of free energy curves are

$$|\Delta F| \sim \begin{cases} \dfrac{N^3\sigma^{7/3}}{R^2} & \text{good solvent} \\ \dfrac{N^3\sigma^3}{R^2} & \theta \text{ solvent} \end{cases} \tag{31}$$

and because $\delta F = \Delta F/F_1$, we can alternatively write

$$|\delta F| \sim \begin{cases} \dfrac{N^2\sigma^{2/3}}{R^2} & \text{good solvent} \\ \dfrac{N^2\sigma}{R^2} & \theta \text{ solvent} \end{cases} \quad (32)$$

Note that the redistribution of the chains from the inner to outer layer does give an additional entropy loss upon bending. This increase in the free energy due to the entropy loss per unit area is given by

$$\Delta F_S = -\sigma[(1+x)\ln(1+x) + (1-x)\ln(1-x)] \quad (33)$$

For a fixed x, this value will not depend on N. Taking eqs 23 and 29 into account, we get a scaling dependence for the low curvature case as

$$|\Delta F_S| \sim \begin{cases} \dfrac{N^2\sigma^{5/3}}{R^2} & \text{good solvent} \\ \dfrac{N^2\sigma^2}{R^2} & \theta \text{ solvent} \end{cases} \quad (34)$$

so for the large N, it becomes negligible compared to the contributions given in eq 31.

Numerical Results and Discussion

In this section we will present results from the numerical SF-SCF calculations. We split this section into two. In the first part, we will consider the structural and thermodynamic effects of curving a quenched brush. In the second part, we will consider the annealed, bilateral brush.

Curved Quenched Polymer Brush. The polymer profiles for the concave and convex brushes at weak curvatures are presented on Figure 3. The discontinuity in profiles is due to the fact that there is no translocation of the chains allowed (the grafting densities on both sides of the plane are fixed $\sigma_+ = \sigma_- = \sigma$ for each brush), and thus the profiles that are computed for two independent cases of concave and convex geometries are put together for comparison with the annealed case.

From Figure 3, one can see that there are strong nonlocal effects present (Figure 3a,b). According to the QP model, the polymer volume fraction in each layer r, irrespective of whether one considers a point on the convex or the concave side, is fully determined by the effective grafting density in that layer (cf. eqs 9 and 18). In this case, the grafting densities for the convex and the concave brushes are fixed and are the same for both sides. However, as evident from the SF-SCF predictions, the polymer volume fractions at the first lattice layers just next to the grafting surface are noticeably asymmetric. The polymer segments of the chains grafted to a convex surface tend to position themselves far from the grafting plane in the exterior of the brush, where they can sample more space. On the concave side, however, there is progressively less space when the segments move away from the grafting plane and as a result the segments are pushed toward the grafting plane. This increases the volume fraction next to the grafting plane. The smaller the R the larger are these effects.

In Figure 5 below, a similar set of graphs is shown for the bilateral (annealed) brush, where the profiles are given for higher curvature (smaller R values). Even though the redistribution was allowed in this case, we still can refer to the volume fraction profiles to discuss how the profiles in general respond to the imposed curvatures.

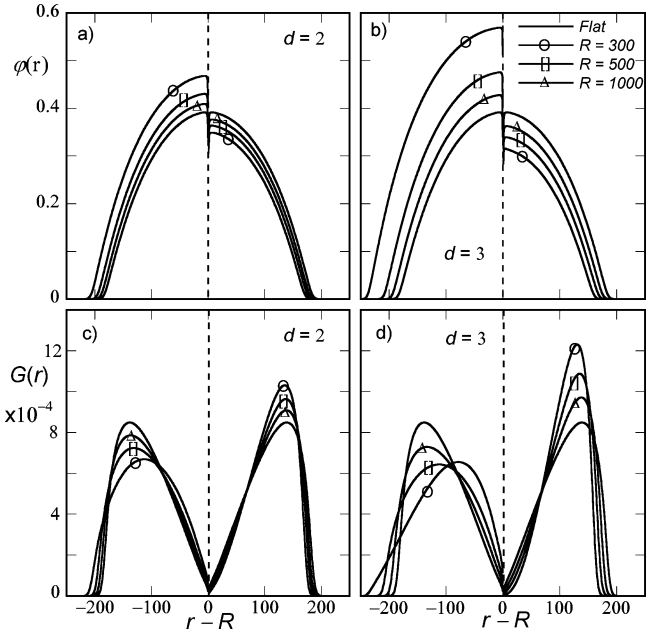

Figure 3. The polymer density profiles $\varphi(r)$ (a,b) and the distribution of free ends $G(r)$ (eq 35) (c,d) for cylindrically curved brushes (a,c) and for spherically curved brushes (b,d) in cases where the redistribution of the polymers is not possible, i.e., the geometrically quenched brush. Besides the flat case, the radii of curvature are $R = 300$, 500, and 1000 as indicated. The chain length is $N = 500$, and the grafting density is $\sigma = 0.1$, and the solvent quality is good ($\chi = 0$). $G(r)$ is normalized to σ, but note that the polymer profile obeys to $N\sigma = \sum_r L(r)\varphi(r)$.

For both brushes with strong and weak curvature, and both on the convex and on the concave sides, the polymer volume fraction profile decreases with distance from surface. For low curvatures as in Figure 3, these profiles are approximately parabolic. In the convex brush with a large curvature (very small values of R as, for e.g., in Figure 5a,b), the radial volume fraction distribution can be divided into two regions. There is a power-law dependence of $\varphi(r)$ for the layers near the grafting surface, and a parabolic-like dependence for the region farther from the grafting surface (i.e., the exterior). The analytical theory of convex brushes (both in the QP and in the NL approximations) describes only the power-law dependence, due to the constraints on the free ends. For weakly curved layers (Figure 3a,b), this power-law dependence is absent, and this illustrates a potential problem for the analytical models.

On the concave side, the profiles are fundamentally different. Again the characteristics are best seen for high curvatures as given in Figures 5a,b. Basically, the decrease of the polymer volume fraction with increasing distance from the grating surface weakens with the increase in the curvature H_1/R. In a limit $H_{in} = R$, the volume fraction profile for the concave layer becomes nearly constant. However, the increase in the volume fraction toward the center of curvature as predicted by QP and even NL theories is not observed. The noted difference between the SF-SCF results and the analytical predictions, as well as the existence of a parabolic part of the density distribution in the convex brush, is largely due to the distribution of free polymer ends. Recall again that in the analytical models these distributions are delta functions.

Panels c and d of Figure 3 (and correspondingly Figure 5c,d) present the distribution of ends $G(r)$ as a function of the distance r from the grafting surface both for spherically as well as for cylindrically curved brushes. The end-point distribution gives the number of end points per unit grafting area. Therefore, $G(r)$ is connected with the corresponding volume fraction distribution

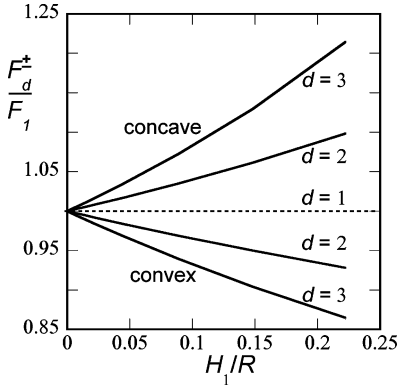

Figure 4. The relative change in free energy $F_d^{\pm}/F_1$, as a function of the relative curvature H_1/R in the weak curvature limit for the quenched (no flip−flop) case. The chain length is $N = 500$, the grafting density is $\sigma = 0.1$, and the solvent quality is good ($\chi = 0$). The cylindrical curvature ($d = 2$) and spherical curvature ($d = 3$) cases are indicated. The horizontal dotted line (labeled $d = 1$) is for the flat geometry (plotted for illustrative purpose only even though there is no R dependence in this case).

Table 3. Coefficients of Free Energy Expansion Found from Equation 23, Fitted from the Numerical SF-SCF Results for the Curved Convex and Concave Brushes[a]

solvent		good		θ solvent	
d	side	a_1	a_2	a_1	a_2
2	+	0.377	0.251	0.52	0.44
	−	0.376	0.254	0.52	0.45
3	+	0.754	0.669	1.03	1.39
	−	0.752	0.731	1.03	1.39

[a] No redistributions of chains, $N = 500$, and $\sigma = 0.1$.

$\varphi(r,N)$ (in the literature often the notation $g(r) \equiv \varphi(r,N)$ is found) by

$$G(r) = \frac{L(r)}{L(R)}\varphi(r,N) \equiv \frac{r^d - (r-1)^d}{R^d - (R-1)^d}\varphi(r,N) \qquad (35)$$

Note that this distribution is normalized to σ, i.e., there are exactly σ end points. As can be seen from Figures 3c,d and 5c,d, with an increase in the curvature (decrease in R), the distribution of free ends tends to shift to the periphery of the brush in the convex layer (toward the parabolic part of density profile) and toward the grafting surface in concave layer. The relative absence of end points near the grafting surface in the strongly curved convex brush is known as the dead zone.[9,32−34] This dead zone is easily observed (near the surface on the convex side) in the Figure 5c,d. In the weak curvature case (Figure 3) the dead zone is absent.

Let us next compare the free energy of the curved brushes as predicted by the SF-SCF method with those given by the analytical models for the good solvent case. The initial part of the free energy curve for the low curvatures is presented in Figure 4, which shows that the change in the free energy is a relative simple function of the curvature parameter. The expansion coefficients a_1 and a_2 for a fit similar to eq 19 are presented in the Table 3. Note that for this expansion it is necessary to determine the height of the brush H_1. In the analytical models, the free ends of the polymer are fixed at the brush exterior, exactly at adistance H_1 from the grafting surface, so that the height is uniquely determined. In the SF-SCF model, however, the free ends are distributed throughout the layer. As a result, there are several options on how to determine the brush height $H_{1(SF)}$ and correspondingly the a_1 and a_2 coefficients.

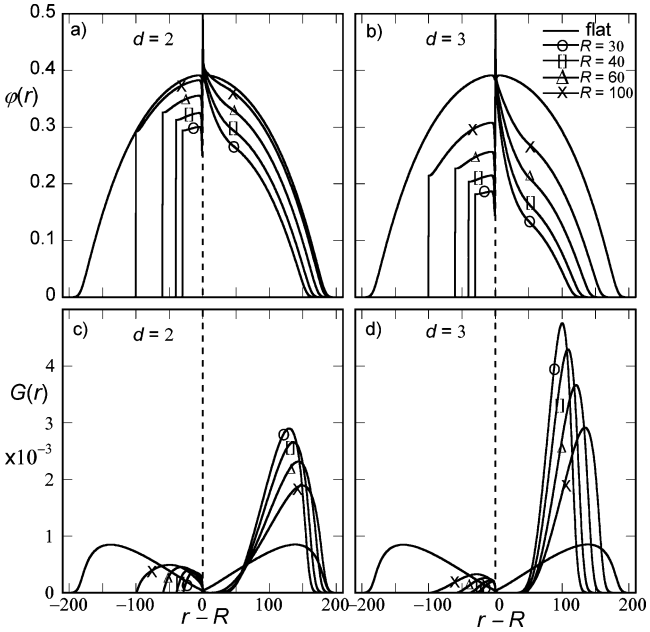

Figure 5. The polymer density profiles $\varphi(r)$ (a,b) and the distribution of free ends $G(r)$ (eq 35) (c,d) for cylindrically curved brushes (a,c) and for spherically curved brushes (b,d) of the annealed bilateral brush. Besides the flat case, the radii of curvature are $R = 30$, 40, 60, and 100 as indicated. The chain length is $N = 500$, the grafting density is $\sigma = 0.1$, and the solvent quality is good ($\chi = 0$). Note that the volume fraction profile trivially becomes zero when $r - R < -R$, i.e., when the r coordinate becomes zero. $G(r)$ is normalized to σ, but note that the polymer profile obeys to $N\sigma = \sum_r L(r)\varphi(r)$.

We will use the first moment of the free ends distribution, $G(r) = \varphi(r,N)$, as a measure for the brush height given by

$$H_{1(SF)} = \frac{\sum_r rG(r))}{\sum_r G(r)} \qquad (36)$$

Comparing the calculated coefficients (Table 3) with the analytical ones (Table 1), we see a reasonable agreement between the analytical methods and the numerical results. To further summarize this part of the study, we present the scaling for the free energy difference ΔF upon bending:

$$\Delta F \sim \begin{cases} \dfrac{N^3\sigma^{2.7}}{R^2} & \text{good solvent} \\ \dfrac{N^3\sigma^{3.3}}{R^2} & \theta \text{ solvent} \end{cases} \qquad (37)$$

which is in good agreement with early scaling predictions[35] and more recent computer simulation studies.[36] The power exponent for the grafting density in good-solvent conditions (2.7) is somewhat larger than that of the scaling prediction ($^7/_3$). This is probably due to the relatively high grafting densities ($0.05 \leq \sigma \leq 0.25$) used in our calculations. We would also like to mention that there is no difference in scaling for bending into spherical or cylindrical geometries. The only differences are in the values of the numerical coefficients.

Bending of a Bilateral Polymer Layer. A selection of the polymer volume fraction profiles and corresponding distributions of free ends for the cylindrically and spherically curved bilateral polymer layers is presented in Figure 5. Again, we present results of the SF-SCF method for a set of curvatures, which are implemented by a set of R values somewhat smaller than that used in Figure 3. We recall that in this case the polymer chains

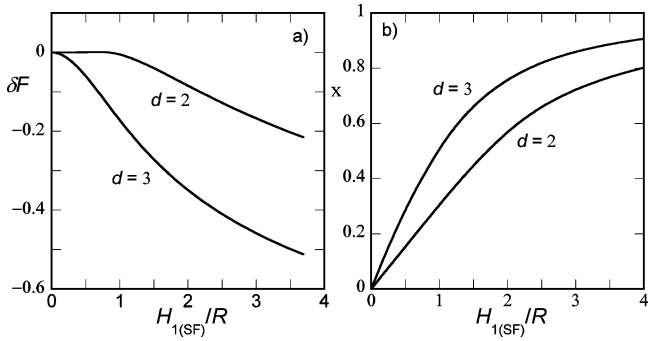

Figure 6. (a) The relative change in the specific free energy upon bending δF as obtained from the SF-SCF model and (b) the fraction of translocated chains x as a function of relative curvature H_1/R for spherical ($d = 3$) and cylindrical ($d = 2$) curvatures. The polymer length is $N = 500$, the grafting density on each side of the grafting plane is $\sigma = 0.1$, and the solvent quality is good ($\chi = 0$.)

are allowed to pass through the layer thereby effectively changing the grafting density of the convex and concave sides. Of course, in this redistribution process, the overall grafting density remains constant. In the limit of very high curvatures, it is found that the volume fractions in the inner (concave) part tend to become independent of the coordinate r; the chains that probe the concave region become highly confined and fill the inner region almost homogeneously. The dependence of the chains redistribution parameter ($x = \Delta\sigma/\sigma$, cf. eq 23) on the curvature parameter ($H_{1(SF)}/R$) is presented in Figure 6b, which may be compared to Figure 2b. For small values of the curvature parameter, the level of redistribution of the chains depends linearly on the curvature parameter (see eq 29), which is similar to the analytical predictions but with a difference in the slopes (for the cylindrical case $b_1 = 0.6$ (analytical) and 0.3 (SCF), and for the spherical case $b_1 = 1.1$ (analytical) and 0.56 (SCF)).

We are now in the position to discuss the main result of this paper. In Figure 6a, we present the numerical result for the change in free energy upon bending for a bilateral brush, i.e., for the annealed case. This result should be compared to the corresponding one in Figure 2a, where the predictions for the QP models were presented. The first impression is that the curves of Figure 6a are similar to those of Figure 2a. For the spherically curved membrane, we find a monotonic decreasing free energy change upon bending, whereas for the cylindrical bending case, there is an initial rise of free energy, similar to that in Figure 2a, followed by a decrease of the free energy at larger curvatures. For spherical bending, this result appears natural and matches the theory independent of the model used. For cylindrical bending, the dependence is indeed nonmonotonous. It is surprising because the NL model predicted a monotonous behavior also for the cylindrical case, which now appears to be qualitatively in conflict with the numerical results. It is necessary to point out that the variation of the free energy in the SF-SCF calculations, at low curvatures, is much weaker than predicted in Figure 2a for both NL and QP models.

A more essential disagreement between the results of Figures 6a and 2a appear when the dependencies of the free energy increase for the cylindrical bending on the governing parameters N and σ are considered. According to the analytical theory the free energy increments for different N and σ values should follow a universal curve in the reduced coordinates of Figure 2a. In Figures 7 and 8, we present these dependencies for the cylindrical and spherical cases as computed from the numerical theory. For the spherically curved bilateral brush, we indeed find a universal dependence; all curves collapse onto one single master curve. In the cylindrical case however, as shown in

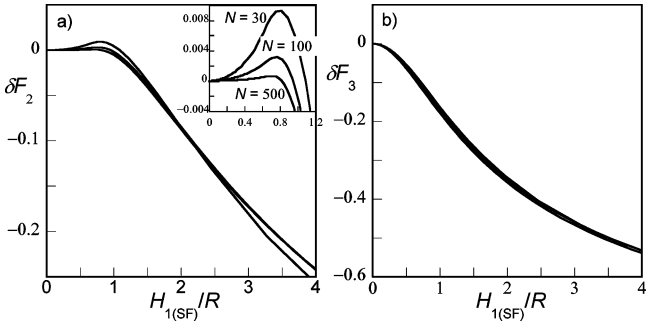

Figure 7. The free energies of curvature for (a) cylindrical and (b) spherical cases calculated with the SF-SCF model for one grafting density $\sigma = 0.25$ and three different chain lengths $N = 30$, 100, and 500. The inset in view graph a demonstrates the initial (low curvature) growth of free energy for the cylindrical bending. Solvent quality is good ($\chi = 0$).

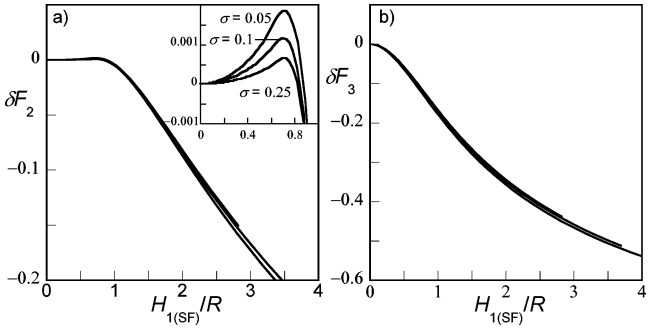

Figure 8. The free energies of curvature for (a) cylindrical and (b) spherical cases calculated with SF-SCF model for one chain length $N = 500$ and three different grafting densities $\sigma = 0.05$, 0.1, and 0.25. The inset in view graph a demonstrates the initial (low curvature) growth of free energy for the cylindrical bending. Solvent quality is good ($\chi = 0$).

Figures 7a and 8a, this is not the case. Close inspection shows that there are pronounced deviations at low curvatures. In the initial positive parts of δF, the relative deviations are important, showing that the dependencies for the various N and σ values definitely do not follow a single master curve as expected in these reduced coordinates.

The scaling dependencies for the increase of ΔF for small curvatures were numerically fitted and found to be given by

$$\Delta F_3 \sim \begin{cases} -\dfrac{N^3\sigma^{2.7}}{R^2} & \text{good solvent} \\ -\dfrac{N^3\sigma^{3.2}}{R^2} & \theta \text{ solvent} \end{cases} \tag{38}$$

for the spherical geometry and for the cylindrical geometry

$$\Delta F_2 \sim \begin{cases} \dfrac{N^{2.1}\sigma^{1.9}}{R^2} & \text{good solvent} \\ \dfrac{N^{2.3}\sigma^{2.3}}{R^2} & \theta \text{ solvent} \end{cases} \tag{39}$$

These results should be compared to similar predictions presented in eqs 31 and 34. In the spherical case, we get a rather satisfactory agreement with the analytical theory. Apparently, the analytical theory correctly accounts the influence of the convex and concave curvatures on interactions and deformation of chains. The positive entropic term (eq 34), due to the redistribution of chains between the layers, is small compared to this relatively large negative term and is not important.

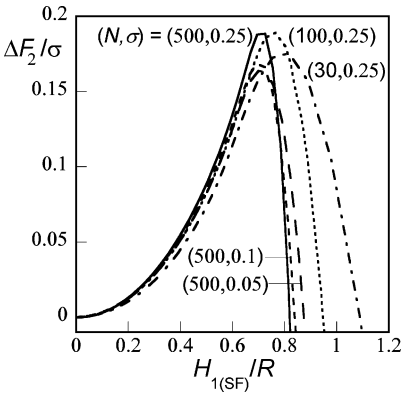

Figure 9. The initial part of the free energy of curvature in the cylindrical geometry normalized per polymer chain, $\Delta F_2/\sigma$ (defined in the text), plotted as a function of the natural measure of the curvature $H_{1(SF)}/R$ as found by the SF-SCF method. The different lines present several chain lengths and grafting densities as indicated. Solvent quality is good ($\chi = 0$).

The opposite situation presents itself for weakly curved layers in the cylindrical geometry. The numerically found ΔF_2 value (eq 39) is much smaller than the theoretical ΔF given in eq 31 (rather it has the magnitude of the entropic term ΔF_S given in eq 34).

Finally, in Figure 9, an additional demonstration of these results is presented. In this figure, we give the free energy of curvature in the cylindrical geometry in the limit of low curvatures, which in this case is normalized per chain, i.e., $F_1\delta F_2/\sigma$. It follows from Figure 9 that the free energy change per chain upon a weak cylindrical bending appears to be a universal function of the relative curvature $H_{1(SF)}/R$. Hence, for weak cylindrical curvatures, one can see only the entropic term ΔF_S, which has masked the ΔF even for $N = 500$. This means that the numerical calculations by the SF-SCF method, which take all the specificity of the bilateral polymer brush into account, give very low values for the b_2 coefficient in eq 30. The question about the sign of this coefficient, which is practically equal to zero, looses sense especially for not too large values of the chain length of the grafted chains. In our calculations, we have restricted ourselves to $N \leq 500$.

Bending Modulus of a Bilateral Polymer Brush. The physics of curved interface is very often put in the perspective of the Helfrich free energy expansion.[37] In this approach, the bending free energy is presented as

$$\Delta F = \int \left(\frac{1}{2}k_c(c_1 + c_2 - 2c_0)^2 + \bar{k}c_1c_2\right) ds \qquad (40)$$

Here the integral is over the whole area of the membrane, $c_1 = 1/R_1$ and $c_2 = 1/R_2$ are the local curvatures in each point, and c_0 is the spontaneous curvature, which is absent in our case due to the symmetry reasons. The bending modulus k_c and the Gaussian modulus $\bar{k}$ can be obtained from considering the homogeneously spherical and homogeneously cylindrical bending cases separately. The free energies per unit area are then expressed as $\Delta F_2 = k_c/2R^2$ and $\Delta F_3 = (2k_c + \bar{k})/R^2$. Thus, we directly translate our scaling predictions to those expected for the mechanical bending rigidities. From the previous expressions 38 and 39, we directly arrive at

$$k_c \sim \begin{cases} N^{2.1}\sigma^{1.9} & \text{good solvent} \\ N^{2.3}\sigma^{2.3} & \theta \text{ solvent} \end{cases} \qquad (41)$$

$$\bar{k} \sim \begin{cases} -N^3\sigma^{2.7} & \text{good solvent} \\ -N^3\sigma^{3.2} & \theta \text{ solvent} \end{cases} \qquad (42)$$

Note that as $\bar{k}$ is much larger in numerical value than k_c its scaling remains similar to the one for ΔF_3 as given in eq 37. We would also like to make a note here that although k_c is positive, which means that the grafted polymer makes the membrane stiffer, it scales almost N times smaller than $\bar{k}$. Therefore, when polymers are long enough, the flat conformation becomes increasingly unstable in favor of bending. From the Helfrich analysis, it is known that the flat conformation remain stable as long as $2k_c + \bar{k} > 0$. When this is no longer the case, i.e., when the chain length is sufficiently large, one should expect nonlamelar geometries such as wormlike or micellar-like objects. Of course, to model these transitions, it becomes necessary to also consider what happens with the rigidity of the surface (membrane) onto which the chains are grafted. Such an analysis is possible in the SF-SCF approach[38−40] but requires a more elaborate model.

Conclusions

The bending of a bilateral symmetrical polymer brush leads to the formation of two inequivalent curved brushes (convex and concave). We have evaluated the free energy of bending of such a membrane when the redistribution of chains from the concave to the convex layer is allowed. Bending of bilateral brushes in the limit of large curvatures is well understood. According to the analytical theory, such brushes stabilize highly curved vesicles from becoming planar. These results are totally confirmed by numerical SF-SCF calculations both for the spherical as well as for the cylindrical type of bending.

For spherical bending, the same situation persists up to the weak curvature regime. The bending free energy in the spherical bending case is negative and monotonically decreases with the imposed curvature. The numerical results obey a universal scaling for the chain length and grafting density dependencies.

The weak cylindrical curvature regime for a bilateral brush differs from the strong curvature limit. As mentioned in the Introduction section, the analytical theory shows contradictory results for a few different approaches. When the free ends are fixed at the external brush boundary, the change ΔF in the conformational free energy of a bilateral brush in the cylindrical mode is positive in the Daoud−Cotton model (QP framework, Birshtein and Zhulina[10]). On the other hand, in the NL framework, $\Delta F < 0$ (see Table 2 and also ref 24). The relaxation of free ends (Subbotin et al.[21]) leads to inversion in sign of ΔF, making the cylindrical mode of curvature unfavorable.

At weak curvatures and for relatively short chains, the conformational contribution, $\Delta F \sim F_1H_1^2/R^2 \sim N^3$, could be comparable to the entropic contribution, $-\Delta F_s \sim H_1^2/R^2 \sim N^2 > 0$, which opposes chain flip−flop from one side of a membrane to the other. The sum of the two terms governs the stability of the flat bilayer at weak cylindrical bending. Clearly, the result is sensitive to both the sign and the value of the numerical coefficient in ΔF. The numerical SF-SCF results, which are expected to be the most realistic, lead to the peculiar conclusion that in the range of molecular weights investigated ($N \leq 500$) the free energy contribution ΔF is in fact close to being nonexistent (the above mentioned coefficient is very small). The modest penalty for the weak cylindrical curvature turned out to be determined by a mere entropic loss due to the redistribution of the chains from one side of the membrane to the other.

Thus, the increase in the free energy caused by the weak cylindrical bending poses just a low and surmountable barrier for the formation of relatively strong and thermodynamically favorable cylindrical curvatures. The other important aspect is that the change in sign of the curvature free energy takes place at $H_1(SF)/R \leq 1$. The bilayer thus retains its ability to bend long before the interactions between oncoming layers on the concave side occurs.

In the Introduction section, we have discussed the connection between the results for the cylindrical bending of an initially flat bilayer and the bending of an adsorbed molecular brush (a comblike polymer). Our numerical results explain the nature of the tendency for such macromolecules to form highly curved structures. A similar situation was found in the solution.[20] Note that, at least qualitatively, the redistribution of side chains in a cross-section of a bent molecular brush in solution resembles to that in a two-dimensional comblike polymer (adsorbed molecular brush). It occurs predominantly from the concave to the convex part of a locally bent macromolecule.

Acknowledgment. The authors acknowledge financial support from the Dutch National Science Foundation (NWO) and the Russian Foundation for Basic Research (RFBR) through a joint project 047.017.026 "Polymers in nanomedicine: design, synthesis, and study of interpolymer and polymer-virus complexes in search of novel pharmaceutical strategies" and partial support from the Russian Foundation for Basic Research (RFBR Grant No. 05-03-33126).

References and Notes

(1) Hiergeist, C.; Lipowsky, R. *J. Phys. II* **1996**, *6*, 1465.
(2) Joannic, R.; Auvray, L.; Lasic, D. D. *Phys. Rev. Lett.* **1997**, *78*, 3402.
(3) Needham, D.; McIntosh, T. J.; Lasic, D. D. *Biochim. Biophys. Acta* **1992**, *1108*, 40.
(4) Marsh, D.; Bartucci, R.; Sportelli, L. *Biochim. Biophys. Acta B* **2003**, *1615*, 33.
(5) Warriner, H. E.; Idziak, S. H. J.; Slack, N. L.; Davidson, P.; Safinya, C. R. *Science* **1996**, *271*, 969.
(6) Birshtein, T. M.; Zhulina, E. B. *Macromol. Theory Simul.* **1997**, *6*, 1169.
(7) Szleifer, I.; Gerasimov, O. V.; Thompson, D. H. *Proc. Natl. Acad. Sci. U.S.A.* **1998**, *95*, 1032.
(8) Rovira-Bru, M.; Thompson, D. H.; Szleifer, I. *Biophys. J.* **2002**, *83*, 2419.
(9) Daoud, M.; Cotton, C. P. *J. Phys.* **1982**, *43*, 531.
(10) Zhulina, E. B. *Polym. Sci. U.S.S.R.* **1984**, *26*, 794.
(11) Birshtein, T. M.; Zhulina, E. B. *Polymer* **1984**, *25*, 1453−1461.
(12) Alexander, S. *J. Phys. Paris* **1977**, *38*, 983.
(13) de Gennes, P. G. *Macromolecules* **1980**, *13* (5), 1069
(14) Zhulina, E. B.; Birshtein, T. M.; Borisov, O. V. *Eur. Phys. J. E* **2006**, *20*, 243.
(15) Birshtein, T. M.; Borisov, O. V.; Zhulina, E. B.; Khokhlov, A. R.; Yurasova, T. A. *Vysokomol. Soedin., Ser. A* **1987**, *29*, 1169.
(16) Fredrickson, G. H. *Macromolecules* **1993**, *26*, 2825.
(17) Saariaho, M.; Ikkala, O.; Szleifer, I.; Erukhimovich, I.; ten Brinke, G. *J. Chem. Phys.* **1997**, *107*, 3267.
(18) Saariaho, M.; Szleifer, I.; Ikkala, O.; ten Brinke, G. *Macromol. Theory Simul.* **1998**, *7*, 211.
(19) Subbotin, A.; Saariaho, M.; Ikkala, O.; ten Brinke, G. *Macromolecules* **2000**, *33*, 3447.
(20) Feuz, L.; Leermakers, F. A. M.; Textor, M.; Borisov, O. *Macromolecules* **2005**, *38*, 8891.
(21) Subbotin, A. de Jong, J.; ten Brinke, G. *Eur. Phys. J. E* **2006**, *20*, 99.
(22) Khalatur, P. G.; Shirvanyanz, D. G.; Starovoitova, N. Y.; Khokhlov, A. R. *Macromol. Theory Simul.* **2000**, *9*, 141.
(23) Khalatur, P. G.; Khokhlov, A. R.; Prokhorova, S. A.; Sheiko, S. S.; Müller, M.; Reineker, P.; Shirvanyanz, D. G.; Starovoitova, N. *Eur. Phys. J. E* **2000**, *1*, 99.
(24) Potemkin, I. I. *Eur. Phys. J. E* **2003**, *12*, 207.
(25) Potemkin, I. I.; Khokhlov, A. R.; Prokhorova, S. A.; Sheiko, S. S.; Müller, M.; Beers, K. L.; Matyjaszewski, K. *Macromolecules* **2004**, *37*, 3987.
(26) Scheutjens, J. M. H. M.; Fleer, G. J. *J. Phys. Chem.* **1979**, *83*, 1619.
(27) Scheutjens, J. M. H. M.; Fleer, G. J. *J. Phys. Chem.* **1980**, *84*, 178.
(28) Evers, O. A.; Scheutjens, J. M. H. M.; Fleer, G. J. *Macromolecules* **1990**, *23*, 5221.
(29) Fleer, G. J.; Cohen-Stuart, M. A.; Scheutjens, J. M. H. M.; Cosgrove, T.; Vincent, B. *Polymers at Interfaces*; Chapman and Hall: London, 1993.
(30) Flory, P. *Principles of Polymer Chemistry*; Cornell University Press: New York, 1953.
(31) De Gennes, P. *Scaling concepts in Polymer Phyics*; Cornell University Press: New York, 1979.
(32) Wijmans, C. M.; Zhulina, E. B. *Macromolecules* **1993**, *26*, 7214.
(33) Semenov, A. N. *Sov. JETP* **1985**, *61*, 733.
(34) Grest, G. S.; Kremer, K.; Witten, N. A. *Macromolecules* **1987**, *20*, 1376.
(35) Milner, S. T.; Witten, T. A. *J. Phys. Paris* **1988**, *49*, 1951.
(36) Laradji, M. *Europhys. Lett.* **2002**, *60* (4), 594
(37) Helfrich, W. *Z. Naturforscher* **1973**, *28c*, 693.
(38) Oversteegen, S. M.; Leermakers, F. A. M. *Phys. Rev. E* **2000**, *62*, 8453.
(39) Claessens, M. M. A. E.; van Oort, B. F.; Leermakers, F. A. M.; Hoekstra, F. A.; Cohen Stuart, M. A. *Biophys. J.* **2004**, *87*, 3882.
(40) Kik, R. A.; Leermakers, F. A. M.; Kleijn, J. M. **2005**, *7*, 1996.

MA071303H